All-experimental analysis of doubly resonant Sum-Frequency Generation spectra for Franck-Condon and Herzberg-Teller vibronic modes

Bertrand Busson

All-experimental analysis of doubly resonant Sum-Frequency Generation spectra for Franck-Condon and Herzberg-Teller vibronic modes

Bertrand Busson[1]

Université Paris-Saclay, CNRS, Institut de Chimie Physique, UMR 8000, 91405 ORSAY, France[a)]

(Dated: 25 April 2022)

The transform technique applied to the analysis of doubly-resonant sum-frequency generation (DR-SFG) spectra is extended to include Herzberg-Teller (HT) vibronic modes. The experimentally measured overlap spectral function generates all the energy resonant amplitudes of the DR-SFG excitation function for both Franck-Condon (FC) and HT modes. When FC modes dominate the DR-SFG spectra, a methodology is provided to perform efficient curve fitting and orientation analysis, in order to extract FC activities of the various vibration modes from experimental spectra with the help of a molecular model. Determination of the FC or HT natures of the vibration modes from DR-SFG data is also shown possible through their visible lineshapes with an appropriate choice of polarizations. As an example, experimental DR-SFG data suggest that a known HT-active mode in the vibronic structure of rhodamine 6G monomers exhibits a FC behavior in molecular aggregates.

[a)]Electronic mail: bertrand.busson@universite-paris-saclay.fr

I. INTRODUCTION

Photo-induced processes take part in numerous applications, triggering chemical reactions[1] or participating in the production of electricity,[2] for example. They often involve charge separation after photo-excitation and production of either electron-hole pairs in a solid state entity (e.g. photovoltaics), or molecular excited states (e.g. photochemistry). They may also involve the transformation of one kind of excitation into another by energy transfer, as happens in plasmon-induced chemistry,[3] photocatalytic chemical reactors for environmental remediation,[4] or inside dye-sensitized solar cells.[5] As these transfers happen at an interface where molecules and their solid state partner coexist and may exchange energy,[6] they rely on a fine tuning of the interaction between both entities.

Taking as an example the molecular side of dye-sensitized solar cells, geometry and orientation in the ground and excited states;[7,8] vibrational, electronic and vibronic structures[9,10] including vibronic coupling; aggregation states;[11] lifetimes and relaxation paths of the involved excited states,[12] all these parameters have to be monitored or controlled at the interface where the processes actually take place in order to improve their efficiency. Both theoretical and experimental investigations show that there is a vibrational or vibronic component involved in the charge transfer mechanism induced by the molecular excitation in the visible range.[12–17] There is therefore a need for non invasive and non destructive tools to monitor as accurately as possible the molecular properties and their link to substrate properties *in situ*, in real time and with a fast dynamics.[12] Among these, doubly-resonant sum-frequency generation spectroscopy (DR-SFG) provides the absolute surface specificity giving straight access to molecular properties at the interface only, getting rid of all the molecular background in the surrounding bulk. Being resonant with vibrational, electronic and vibronic transitions, it possesses the energy resolution needed to selectively probe the elementary processes chosen by the experimenters. Its tensorial nature and specific selection rules make it also sensitive to the absolute orientation of chemical groups and electron density towards the interface, resolved by tuning polarizations of light[7,18] or analyzing peak intensity ratios.[19] Finally, timescales of ultrafast phenomena become accessible using ultrashort laser pulses while adjusting time delays.[20]

DR-SFG setups with tunable visible lasers remain rare in spite of the variety of applications of such experiments available in the literature: chiral response of coupled

oscillators[21–27], vibrational and electronic structures of chromophores[16,28–33] and conjugated polymers,[34,35] charge transfer states induced by molecular adsorption on metals.[36–42] One of the reasons for this sparseness may be that, as for resonant Raman scattering, data interpretation is made difficult by several aspects. i) The selection rules for double resonance of a vibration mode depend on the nature of the vibronic activity of this mode. Franck-Condon (FC) active modes are straightforwardly DR-SFG active, but FC-inactive ones may still acquire DR-SFG activity through vibronic coupling to another mode by a Herzberg-Teller (HT) mechanism.[43,44] The question whether FC and non-FC mode intensities may compare in an experimental spectrum is still open in spite of a few results tending to prove that it should be possible in some cases.[33,45] ii) It is rather simple to predict the theoretical DR-SFG lineshape of a vibration mode when electron-vibration coupling is supposed linear in the vibration coordinates.[46–48] However, it is well-known from resonant Raman literature that quadratic coupling terms may alter the intensities and profiles of vibrations when they cannot be neglected.[49] iii) Even in the linear coupling scheme, the DR-SFG activity involves the whole molecular vibronic structure through FC overlap integrals. Predicting the DR-SFG activity, for example from first-principle calculations,[45] supposes to take this complete structure into account, or to add hypotheses to drastically simplify the theory.[34] iv) The theory predicts that the vibrational Lorentzian functions generating a DR-SFG spectrum do not share a common phase, as is usually the case for singly-resonant SFG experiments,[19] adding a difficulty in the fitting step of the experimental data.[50] In order to come over these issues, we have introduced in a previous paper the overlap spectral function formalism.[17] It allows to skip point iii) by including the whole vibronic activity into a single function Φ of the visible energy, which is in addition extracted from elementary experimental absorption data. Moreover, quadratic coupling phenomena mentioned in point ii) appear as higher order terms which still factorize into sums of Φ functions.[48,49]

In this paper, we propose to build on the overlap spectralfunction formalism to address the remaining points i) and iv). Specifically, we show that Φ is also well adapted to describe the amplitude lineshapes of HT modes in a DR-SFG spectrum, important as vibronic coupling plays a role in the electron injection processes.[12] Interestingly, the predicted lineshapes for HT modes fundamentally differ from FC modes, and should allow clear experimental determination of the FC or HT natures of the vibration modes from their excitation spectra. We also provide some direct tools dedicated to the curve fitting procedures and orientational

analysis of the DR-SFG spectra (point iv), in order to guide future users to extract reliable and useful data from their experimental spectra.

II. MICROSCOPIC DR-SFG RESPONSE

In a single infrared-visible DR-SFG process, the whole vibrational and vibronic structure of the molecule may be probed in a resonant manner. The infrared photon induces a change in vibrational quantum number for vibration mode l and a jump to the first vibrational level of the ground state. From there, the visible photon induces a second jump towards the vibronic structure, potentially resonant with any vibronic mode of the excited state, in accordance with the photon energy and vibronic selection rules. We may separate these selection rules in two families. In the first one, the Condon approximation is valid, meaning that the electronic jump induced by the visible photon is so fast that the nuclei don't have time to move. As consequences, the electronic transition dipole moment does not depend on the vibration coordinates and is considered as a constant μ_{eg}^0, the electronic jump is vertical. Within this approximation, the activity of a vibronic mode is evaluated by the Franck-Condon (FC) overlap between the vibrational parts of the wavefunctions in the ground and excited states. As many overlap integrals do not vanish, the number of modes involved is rather significant. In the second family, vibronic coupling is taken into account in a Herzberg-Teller (HT) process. This time, the electronic transition moments is supposed to depend on the vibration coordinate of some vibration modes. This induces an extra activity of these modes beyond (or in place of) their FC activity, and allows for coupling between vibronic states, leading to intensity borrowing from HT-active modes by other modes.

In a very general way, the molecular doubly resonant SFG hyperpolarisability may be written as:[48]

$$\beta_{\alpha\beta\gamma}(\omega_{\mathrm{SFG}},\omega_{\mathrm{IR}},\omega_{\mathrm{vis}}) = 1/\hbar^2 \sum_l \frac{\Big[FC\Big]_l^{\alpha\beta\gamma} + \sum_{p=1}^{3}\Big[HT_p\Big]_l^{\alpha\beta\gamma}}{\omega_{IR}-\omega_l+i\Gamma_l}, \tag{1}$$

where α, β, γ stand for Cartesian coordinates in the molecular frame and summation $\{l\}$ runs over the IR-active modes. The first term at the numerator stands for the Franck-Condon amplitude. The others (HT1, HT2, HT3) represent the first three components of the Herzberg-Teller contribution. They involve vibronic couplings between mode l and all

HT-active modes, including itself if relevant.

$$\Big[FC\Big]_l^{\alpha\beta\gamma} = A_l^{\alpha\beta\gamma} D_l(\omega_{SFG}) \tag{2}$$

$$\Big[HT_1\Big]_l^{\alpha\beta\gamma} = \sum_a^{HT-active} B_{1,l,a}^{\alpha\beta\gamma} E_{1,l,a}(\omega_{SFG}) \tag{3a}$$

$$\Big[HT_2\Big]_l^{\alpha\beta\gamma} = \sum_a^{HT-active} B_{2,l,a}^{\alpha\beta\gamma} E_{2,l,a}(\omega_{SFG}) \tag{3b}$$

$$\Big[HT_3\Big]_l^{\alpha\beta\gamma} = \sum_{a,b}^{HT-active} B_{3,l,a,b}^{\alpha\beta\gamma} E_{3,l,a,b}(\omega_{SFG}) \tag{4}$$

All these terms consist of a static amplitude A_l or B_l, carrying the $(\alpha\beta\gamma)$ components of the molecular transition dipole moments in the molecular frame, multiplied by an excitation spectrum $D_l(\omega_{SFG})$ or $E_l(\omega_{SFG})$ responsible for the energy resonances between the optical processes and the electronic and vibronic transitions. For all terms, these energy lineshapes are therefore separated from the mode activities and molecular geometry. These functions $D_l(\omega)$ and $E_l(\omega)$ (and, by extension, the part of the experimental DR-SFG amplitude of a vibration mode which varies with the visible color) will be equally called excitation spectra or visible lineshapes in the following.

Expanding the electronic transition dipole moment between ground state (g) and excited state (e) gives

$$\boldsymbol{\mu}_{eg} = \boldsymbol{\mu}_{eg}^0 + \sum_a \left(\frac{\partial \boldsymbol{\mu}_{eg}}{\partial Q_a}\right)_0 Q_a, \tag{5}$$

where the static moment at equilibrium μ_{eg}^0 fulfils the Condon approximation and is therefore responsible for the FC-response. The other terms represent the first-order deviation to this approximation, giving rise to the HT contribution. The summation is effectively restricted to the vibration modes with HT activity, i.e. for which $\left(\frac{\partial \boldsymbol{\mu}}{\partial Q_a}\right)_0$ does not vanish. We have:

$$A_l^{\alpha\beta\gamma} = \mu_{eg}^{0,\alpha} \mu_{eg}^{0,\beta} \left(\frac{\partial \mu^\gamma}{\partial Q_l}\right)_0 \tag{6}$$

where the last term is the IR activity of mode l. The HT amplitudes are given by:

$$B_{1,l,a}^{\alpha\beta\gamma} = \mu_{eg}^{0,\alpha} \left(\frac{\partial \mu_{eg}^\beta}{\partial Q_a}\right)_0 \left(\frac{\partial \mu^\gamma}{\partial Q_l}\right)_0 \tag{7}$$

$$B_{2,l,a}^{\alpha\beta\gamma} = \left(\frac{\partial \mu_{eg}^\alpha}{\partial Q_a}\right)_0 \mu_{eg}^{0,\beta} \left(\frac{\partial \mu^\gamma}{\partial Q_l}\right)_0 \tag{8}$$

$$B^{\alpha\beta\gamma}_{3,l,a,b} = \left(\frac{\partial \mu^{\alpha}_{eg}}{\partial Q_a}\right)_0 \left(\frac{\partial \mu^{\beta}_{eg}}{\partial Q_b}\right)_0 \left(\frac{\partial \mu^{\gamma}}{\partial Q_l}\right)_0 \tag{9}$$

There is no unique definition of the so-called Herzberg-Teller contribution, as it has evolved over fifty years of literature. Some authors consider HT1 and HT2 as mixed FC/HT terms, and HT3 as the pure HT contribution.[43] On the contrary, some others limit the Herzberg-Teller contributions to the first order in Q-dependency, thus to HT1 and HT2.[45,51] Finally, the name Herzberg-Teller sometimes refers to all three terms, as we do here, and HT1 and HT2 are considered as the first two HT terms.[33] Many publications also simply separate the DR-SFG response into A and B contributions, referring (explicitly or not) to FC and HT terms, respectively.[24,52] This formalism originates in the Raman analysis by Albrecht,[53] where A, B and C refer to FC, HT1/2 and HT3, respectively. Finally, a subsequent publication by the same author, explicitly relying on the transform technique formalism, modified these into generalized A, B and C, referring to FC, HT1 and HT2, respectively.[54]

As for the excitation lineshapes D_l and E_l in Eq. 2-4, the FC response has been calculated in the harmonic oscillator frame, taking into account several degrees of complexity of the vibronic structure. In the excited state, the vibronic eigenmodes differ in general from the vibrational ones in the ground state as a result of mode distortion (implying a change in the vibration frequencies) and Duschinsky rotation (leading to mode mixing) induced by quadratic electron-vibration coupling terms in the hamiltonian describing the excited state. When these two effects are fully taken into account at arbitrary temperature, the resulting $D_l(\omega)$ is given in integral form in Ref. 55. For low amplitude mode distortions and low angle mode mixing limited to an arbitrary number of pairs of modes, these effects appear as a higher-order perturbation of the linear electron-vibration coupling situation and the expression of $D_l(\omega)$ at vanishing temperature may be simplified to the first order into:[48,49]

$$D_l(\omega) = D_l^{DIS}(\omega) + D_l^{\theta}(\omega) + D_l^{CT}(\omega) \tag{10}$$

where $D_l^{DIS}(\omega)$ stands for the excitation spectrum in the distorted vibronic structure, $D_l^{CT}(\omega)$ for the corrective term due to mode mixing involving mode l, and $D_l^{\theta}(\omega)$ for the corrective term due to mode mixing of all other vibronic modes. These excitation spectra are conveniently factorized by the introduction of the overlap spectral function $\Phi(\omega)$ according to the expressions recalled in Ref. 48. This function $\Phi(\omega)$ may be deduced from absorbance

measurements

$$A(\omega) \propto \omega \left|\mu_{e\leftarrow g}\right|^2 \mathrm{Im}\left[\Phi(\omega)\right], \tag{11}$$

where A is the molecular absorbance, in order to recover the spectral shape of the excitation function $D_l(\omega_{SFG})$.[17] The essential vibronic parameters are the shifts Δ_l in the harmonic potential wells along the normal mode coordinate Q_l of mode l. Using either linear or quadratic electron-vibration coupling, the FC activity of mode l is essentially determined and quantified by the value of Δ_l. When this quantity vanishes, the mode is FC-inactive, except from a potential small contribution due to coupling with another FC-active mode through mode mixing.[48,49] At the lowest order of approximation, i.e. linear electron-vibration coupling, Δ_l fully drives the FC-activity, and we have:

$$D_l\left(\omega_{SFG}\right) = \frac{\Delta_l}{2}\left[\Phi\left(\omega_{SFG}\right) - \Phi\left(\omega_{SFG} - \omega_l\right)\right] \tag{12}$$

It has been shown[17] that the experimental visible lineshape for a FC mode follows indeed this equation.

The HT contribution has been less studied for application to DR-SFG[24,26,33,45] but is well known in the resonance Raman spectroscopy community, which has developed a methodology to integrate it into the RRS formalism and other nonlinear phenomena.[43] It is in principle possible to introduce quadratic electron-vibration coupling phenomena at the HT level of theory.[56] However, as the HT terms already represent a first-order correction to FC terms, we may safely neglect these higher order contributions and stick to the linear coupling scheme. Details on the implementation of HT terms into the overlap spectral function formalism are provided in the Appendix.

We get for the excitation functions:

$$E_{1,l,a}(\omega) = \frac{\Delta_l}{2}\frac{\Delta_a}{2}\left[-\Phi(\omega) + \Phi(\omega-\omega_l) + \Phi(\omega-\omega_a) - \Phi(\omega-\omega_l-\omega_a)\right] - \frac{\hbar}{2\omega_l}\Phi(\omega)\delta_{al} \tag{13}$$

$$E_{2,l,a}(\omega) = \frac{\Delta_l}{2}\frac{\Delta_a}{2}\left[-\Phi(\omega) + \Phi(\omega-\omega_l) + \Phi(\omega-\omega_a) - \Phi(\omega-\omega_l-\omega_a)\right] - \frac{\hbar}{2\omega_l}\Phi(\omega-\omega_l)\delta_{al} \tag{14}$$

$$
\begin{aligned}
E_{3,l,a,b}(\omega) = \frac{\Delta_l}{2}\frac{\Delta_a}{2}\frac{\Delta_b}{2}\,[&\Phi(\omega) - \Phi(\omega-\omega_l) - \Phi(\omega-\omega_a) - \Phi(\omega-\omega_b) \\
&+ \Phi(\omega-\omega_l-\omega_a) + \Phi(\omega-\omega_l-\omega_b) + \Phi(\omega-\omega_a-\omega_b) - \Phi(\omega-\omega_l-\omega_a-\omega_b)] \\
&+ \frac{\hbar\Delta_l}{4\omega_a}\left[\Phi(\omega-\omega_a) - \Phi(\omega-\omega_a-\omega_l)\right]\delta_{ba} + \frac{\hbar\Delta_b}{4\omega_l}\left[\Phi(\omega-\omega_l) - \Phi(\omega-\omega_l-\omega_b)\right]\delta_{al} \\
&+ \frac{\hbar\Delta_a}{4\omega_l}\left[\Phi(\omega) - \Phi(\omega-\omega_a)\right]\delta_{bl}
\end{aligned}
\tag{15}
$$

After determining function $\Phi(\omega)$ of the system once for all,[17] all the HT excitation spectra for mode l become available with a minimal amount of parameters, namely shift Δ_l, and those for the selected HT-active modes Δ_a and Δ_b. As the FC activity of mode l is essentially determined and quantified by the value of Δ_l, this shows that the FC and HT activities are not completely independent, i.e. all FC-active modes have a HT contribution to their excitation lineshapes by coupling to a HT-active mode a. In the HT excitation spectra, most of the terms are indeed proportional to Δ_l, and therefore vanish only for a FC-inactive mode l. In the same way, as HT-activity of mode l relies on its coupling to a and b modes, these must be both HT- and FC-active to contribute. The only exception lies in the self-coupling terms (proportional to δ_{al}) in Eq. 13 and 14, through which mode l contributes to its own DR-SFG excitation function at the HT level as long as it exhibits a non-Condon nature, and whatever its FC-activity.

Equations 1 to 15 provide the full molecular DR-SFG response using a minimal amount of approximations. However, the various terms listed in Eq. 10 to 15 don't have the same order of magnitude. The FC-terms have been studied in details:[48,49] in the linear electron-vibration coupling approximation (as is usually seen in the literature at either arbitrary[46,47] or vanishing[17] temperature), they represent the lowest order of perturbation and, thus, the dominant terms. Contributions due to mode distortion and mode mixing are higher-order perturbations (i.e. increasing powers of the Huang-Rhys factors $S_j = \frac{\omega_j(\Delta_j)^2}{2\hbar}$) of the lowest order. In the same way, the HT-terms arise from a perturbation, through the $\left(\frac{\partial\mu_{eg}}{\partial Q_a}\right)_0$ coupling constants, of the lowest order represented by the μ^0_{eg} factors. In this way, keeping only the lowest order of perturbation, the E_3 contribution may be neglected as a second order term. In the E_1 and E_2 functions, the generic terms also appears as a higher order term, of the order of S_j. As a consequence, the lowest order term for the whole HT development only lies in the self-coupling contributions in E_1 and E_2 (i.e. the last terms in Eq. 13 and

14).

To summarize this discussion, when neglecting all the higher order contributions, the excitation spectrum of mode l dramatically simplifies and involves four terms, each one proportional to Φ function evaluated at a particular energy:

$$\beta_{\alpha\beta\gamma} = 1/\hbar^2 \sum_l \frac{\left(\frac{\partial\mu^\gamma}{\partial Q_l}\right)_0}{\omega_{IR} - \omega_l + i\Gamma_l} \left\{ \mu_{eg}^{0,\alpha}\mu_{eg}^{0,\beta}\frac{\Delta_l}{2}\left[\Phi(\omega_{SFG}) - \Phi(\omega_{SFG} - \omega_l)\right] \right. \\ \left. -\frac{\hbar}{2\omega_l}\left[\mu_{eg}^{0,\alpha}\left(\frac{\partial\mu_{eg}^{\beta}}{\partial Q_l}\right)_0 \Phi(\omega_{SFG}) + \left(\frac{\partial\mu_{eg}^{\alpha}}{\partial Q_l}\right)_0 \mu_{eg}^{0,\beta}\Phi(\omega_{SFG} - \omega_l)\right]\right\}. \tag{16}$$

When the mode is FC-active, the first two terms dominate, and the last two (HT-terms) represent a small perturbation to the well-known FC excitation spectrum.[46] When the mode is FC-inactive, the HT-terms are the only contribution at the lowest order of perturbation. Amplitude of mode l in this case should be overwhelmed by the amplitudes of neighbouring FC-active modes,[26] but it may happen that it remains among the most intense in the DR-SFG spectrum, when its infrared activity is high enough to compensate for the low excitation function or has favourable components along IR beam polarization,[45] or when the choice of the visible wavelength favors double resonance of the HT modes rather than FC ones.[33]

III. MACROSCOPIC DR-SFG RESPONSE OF AN ISOTROPIC THIN FILM

Having evaluated the hyperpolarizability $\alpha\beta\gamma$ component in the molecular frame, we now turn to the macroscopic nonlinear response. The SFG intensity $I(\omega_{IR}, \omega_{vis})$ is equal to

$$I(\omega_{IR}, \omega_{vis}) = \frac{8\pi^3\omega_{\mathrm{SFG}}^2}{c^3\cos^2\theta_{\mathrm{SFG}}}|\chi_{\mathrm{eff}}^{(2)}|^2 I_{\mathrm{vis}} I_{\mathrm{IR}} \tag{17}$$

where the effective nonlinear susceptibility $\chi_{eff}^{(2)}$ is a linear combination of (i,j,k) components $\chi_{ijk}^{(2)}$ in the (x,y,z) laboratory frame, weighted by local field factors,[19] which may be explicitly calculated, and $\chi_{ijk}^{(2)} = \frac{N_s}{\varepsilon_0}\langle\beta_{\alpha\beta\gamma}\rangle$ where N_s is the surface density of molecules, $\beta_{\alpha\beta\gamma}$ the molecular hyperpolarisability in a molecular frame (a,b,c) and the angle brackets average over molecular orientations.[57] When the SFG process takes place at an isotropic (x,y) thin film, it is well-known that only xxz=yyz, xzx=yzy, zxx=zyy and zzz components survive the averaging step. For s-polarization of light aligned along y, these components follow the conventional correspondence between ssp and yyz; sps and yzy; pss and zyy, whereas ppp is

a combination of xxz, xzx, zxx and zzz. Averaging is conveniently performed by considering distributions over molecular Euler angles (ψ, θ, ϕ), namely:

$$\chi^{(2)}_{ijk} = \frac{N_s}{\varepsilon_0} \sum_{\alpha\beta\gamma} \langle D_{i\alpha} D_{j\beta} D_{k\gamma} \rangle \beta_{\alpha\beta\gamma} \tag{18}$$

where matrix **D** gathers the projections of the molecular frame vectors onto the laboratory basis.[58,59] In an isotropic thin film on a solid substrate, it is usually considered that the molecular tilt (θ) and twist (ψ) angles are fixed.[45] The detailed expression of Eq. 18 in this case as a function of θ and ψ may be found in the literature.[60,61] Molecules at the surface of water show a broader distribution of θ and ψ angles.[26] For terminal methyl vibrations of an alkyl chain, or for uniaxial molecular symmetry in general, averaging over ψ is sometimes also considered, provided that c is aligned with the symmetry axis.[62] In these isotropic conditions, there are no anisotropic molecular interactions and all molecules therefore share the same single electronic transition.

Experimentally, a series of vibrational spectra, $I(\omega_{IR}, \omega_{vis})$ as a function of ω_{IR} with fixed ω_{vis}, is recorded while selecting several values for ω_{vis}. Each vibrational spectrum is in general described by Eq. (17), (18) and (1). The challenge lies first in extracting the energy and amplitude of each mode from the experimental data, then linking the amplitudes to the relevant molecular parameters (transition dipole moments, vibration shifts) in order to finally deduce the molecular orientation in the films. We show how to proceed when only FC-active modes are present in the spectra, then consider also the presence of HT-modes.

A. All modes FC active

1. Principles

When all modes l in a spectrum are FC-active, the hyperpolarizability components become:

$$\chi^{(2)}_{ijk} = \sum_l \frac{\Phi(\omega_{SFG}) - \Phi(\omega_{SFG} - \omega_l)}{\omega_{IR} - \omega_l + i\Gamma_l} \chi^l_{ijk} \tag{19}$$

with

$$\chi^l_{ijk} = \frac{N_s}{2\varepsilon_0 \hbar^2} \Delta_l \sum_{\alpha\beta\gamma} \langle D_{i\alpha} D_{j\beta} D_{k\gamma} \rangle A^{\alpha\beta\gamma}_l \tag{20}$$

where the static amplitude $A^{\alpha\beta\gamma}_l$ of each mode l is given by Eq. 6, and χ^l_{ijk} are real numbers. We note that the electronic transition moments in $A^{\alpha\beta\gamma}_l$ are symmetric in α and β, with

the consequence that ijk and jik components of $\chi^{(2)}$ become equal,[62] and in the isotropic case we have $zyy = yzy$. We recover the rule applicable to singly-resonant SFG (SR-SFG, i.e. far from an electronic resonance), where the Raman tensor is symmetric in α and β as soon as molecular chirality does not come into play.[22,63] There are only three independent $\chi^{(2)}$ components left in the macroscopic response. We see that each D_l lineshape (Eq. 12) is common to all hyperpolarizability components and therefore transfers to the macroscopic response,[49] as has been shown experimentally on ssp and ppp visible lineshapes of rhodamine films.[17]

As there is now a separation as a product between the energy lineshapes and molecular amplitudes, it becomes possible to calculate on one side the visible lineshape $\Phi(\omega_{SFG}) - \Phi(\omega_{SFG} - \omega_l)$, and extract on the other side the IR lineshape by fitting the vibrational spectra to a sum of Lorentzian functions. After this curve fitting step, amplitude χ^l_{ijk} for each vibration l is a linear combination of real factors $A_l^{\alpha\beta\gamma}\Delta_l$. For DR-SFG used as a chemical probe of the interface, the important parameters are vibrational frequencies and widths,[38] or the evolution of Lorentzian amplitudes as a function of the visible color,[35] and such a curve fitting may suffice.

To go further into tensorial analysis, we note that the electronic part of the hyperpolarizability tensor (i.e. indexed by α and β) does not depend on the vibration mode l, but only on the α and β components of the electronic transition moments and on constant parameter Δ_l. This fundamentally differs from the usual SR-SFG case,[61,64] for which this electronic part is proportional to the $\alpha\beta$ component of the Raman tensor of mode l. Consequently, orientation analysis for DR-SFG relies separately on the projections of electronic transition dipoles $\mu_{eg}^{0,\alpha}\mu_{eg}^{0,\beta}$ and vibrational activities $\left(\frac{\partial\mu^\gamma}{\partial Q_l}\right)_0$, and not on molecular $\left(\frac{\partial\alpha^{\alpha\beta}}{\partial Q_l}\right)_0$ as for SR-SFG.[57] In a DR-SFG spectrum, different vibration modes share common μ_{eg}^0 components but differ in Δ_l and $\left(\frac{\partial\mu^\gamma}{\partial Q_l}\right)_0$, while, for different polarization combinations, a given vibration mode has a constant Δ_l but $\mu_{eg}^{0,\alpha}$, $\mu_{eg}^{0,\beta}$ and $\left(\frac{\partial\mu^\gamma}{\partial Q_l}\right)_0$ components differ.

For vibrational SR-SFG, the molecular frame (a,b,c) is typically set according to molecular symmetries, in order to reduce the number of nonvanishing β components. The essential quantities like $\left(\frac{\partial\mu^\gamma}{\partial Q_l}\right)_0$ are therefore deduced or calculated in this frame, where they also benefit from the symmetry properties, and the SFG spectra simulated as functions of θ and ψ.[65–67] Here we proceed in a different way by first choosing (c) axis along the molecular electronic transition moment, that is $\mu_{eg}^{0,a} = \mu_{eg}^{0,b} = 0$.[68] For a symmetric molecule, the ori-

entation of its transition dipole moments is linked to its symmetry elements, and so is axis (c). However, we present a general methodology valid for C_1 molecules, which means that all μ vectors have three independent nonvanishing components in the general case. We also choose the direction of axis c to get $\cos\theta \geq 0$, which fixes the quadrant of θ. At this stage, only components β_{cca}, β_{ccb} and β_{ccc} remain, from which $\left|\mu_{eg}^{0,c}\right|^2$ may be factored. Again, for a molecule with a high symmetry, components β_{cca} and β_{ccb} may vanish, which substantially simplifies the analysis.[68]

Following Eq. 19 and 20, we have:

$$\chi^l_{yzy} = \chi^l_{zyy} = \frac{N_s \Delta_l}{2\epsilon_0 \hbar^2} \sin\theta\cos\theta \left[A_l^{ccc}\sin\theta + A_l^{cca}\cos\theta\cos\psi - A_l^{ccb}\cos\theta\sin\psi\right] \tag{21}$$

$$\chi^l_{yyz} = \frac{N_s \Delta_l}{2\epsilon_0 \hbar^2} \sin^2\theta \left[A_l^{ccc}\cos\theta - A_l^{cca}\sin\theta\cos\psi + A_l^{ccb}\sin\theta\sin\psi\right] \tag{22}$$

$$\chi^l_{zzz} = \frac{N_s \Delta_l}{\epsilon_0 \hbar^2} \cos^2\theta \left[A_l^{ccc}\cos\theta - A_l^{cca}\sin\theta\cos\psi + A_l^{ccb}\sin\theta\sin\psi\right] \tag{23}$$

It appears that χ^l_{yyz} is proportional to χ^l_{zzz} (and conversely $\chi^{(2)}_{yyz}$ to $\chi^{(2)}_{zzz}$) by a geometric factor $\dfrac{\sin^2\theta}{2\cos^2\theta}$ corresponding to the $\left(\mu_{eg}^{0,y}\right)^2 / \left(\mu_{eg}^{0,z}\right)^2$ ratio. In the same way, we have two relationships between yzy and yyz, namely:

$$\sin^2\theta\chi^l_{yzy} + \cos^2\theta\chi^l_{yyz} = \frac{N_s \Delta_l}{2\epsilon_0 \hbar^2} \sin^2\theta\cos\theta \left|\mu_{eg}^{0,c}\right|^2 \left(\frac{\partial\mu^c}{\partial Q_l}\right)_0 \tag{24}$$

and

$$\chi^l_{yzy} - \chi^l_{yyz} = \frac{N_s \Delta_l}{2\epsilon_0 \hbar^2} \sin\theta \left[A_l^{cca}\cos\psi - A_l^{ccb}\sin\psi\right] \tag{25}$$

where, for each mode l:

$$A_l^{cca}\cos\psi - A_l^{ccb}\sin\psi = \left|\mu_{eg}^{0,c}\right|^2 \left[\left(\frac{\partial\mu^a}{\partial Q_l}\right)_0 \cos\psi - \left(\frac{\partial\mu^b}{\partial Q_l}\right)_0 \sin\psi\right] \equiv \left|\mu_{eg}^{0,c}\right|^2 \left(\frac{\partial\mu^\psi}{\partial Q_l}\right)_0 \tag{26}$$

and $\left(\frac{\partial\mu^\psi}{\partial Q_l}\right)_0$ corresponds to the projection of $\left(\frac{\partial\mu^\perp}{\partial Q_l}\right)_0$, the IR dipole moment component in the (a,b) plane, onto $\psi = 0$ axis (i.e. the (a) axis before ψ rotation). There are in fact four unknown parameter for each mode l, namely Δ_l and the three $\left(\frac{\partial\mu^\gamma}{\partial Q_l}\right)_0$ coordinates, in addition to θ and ψ common to all modes, whereas only two independent equations remain. Additional input, either experimental or computed, is therefore necessary.

2. Practical implementation

Tilt angle θ accounts for the projection from (c) to (z), and it is easy to show that $\left(\mu_{eg}^{0,y}\right)^2 = \frac{1}{2}\left(\mu_{eg}^{0,c}\right)^2 \sin^2\theta$ and $\left(\mu_{eg}^{0,z}\right)^2 = \left(\mu_{eg}^{0,c}\right)^2 \cos^2\theta$.[58,69] By comparing *in situ* maximal absorbance on oblique incidence with s- and p-polarized light (accounting for Fresnel reflectivity correction) or by rotating the film,[70] θ is experimentally determined, and we deduce the $\chi^{(2)}_{yyz}$ to $\chi^{(2)}_{zzz}$ ratio. Resonant second order nonlinear optical techniques like Second Harmonic Generation or Electronic Sum-Frequency Generation,[71,72] more elaborate and more sensitive to the monolayer level, may even prove more efficient to provide valuable information on tilt angle θ and the electronic part of the phenomenon in general. At this stage, it becomes helpful to involve a molecular model in the analysis, from which the orientation of the electronic transition dipole moment may be estimated. This model may follow from first principle calculations (e.g. geometry optimization and vibration mode calculation by DFT), but even a simpler and more flexible ball-and-stick model of the molecular structure may be sufficient, provided that it is complemented with some spectroscopic data. Orientation analysis amounts to adjusting θ and ψ angles to match the model with the experimental data, in a first step the knowledge of θ makes it possible to orient the (c) axis of the molecular model[73,74] with respect to the surface. The value of ψ is still undetermined, which means that axes (a) and (b) may rotate freely around (c), or that there is no fixed orientation for the molecule as for the (c)-rotation.

Recording and fitting DR-SFG spectra with sps, ssp and ppp polarization combinations suffices to carry out the analysis described in part III A 1, as detailed below. For SR-SFG, it is sometimes difficult to measure sps and pss polarization combinations due to low signal levels.[61,75,76] Here, specific enhancements due to the double resonance should lead to better signal-to-noise ratios. The χ^l_{ijk} components have to be separated in the three experimental spectra by curve fitting. In conventional SFG data analysis, vibrational spectra are fitted by a sum of complex Lorentzian functions as a function of ω_{IR} with constant amplitudes A_l, the unknown parameters being ω_l, Γ_l and A_l. For DR-SFG (Eq. 16), the FC amplitudes also depend on ω_l and ω_{IR} through D_l (Eq. 1 and 12), which means that their spectral dependence slightly varies from mode to mode, that they are not constant over the vibrational spectrum and that they each possess a distinct phase,[49] all this being often simplified in the literature.[28] From Eq. (11), function $\Phi(\omega)$ is first deduced from a single *in situ* absorption measurement

followed by a Kramers-Kronig transformation,[17] then used as an input in the curve fitting procedure. The knowledge of $\Phi(\omega)$ makes it in principle possible to calculate the amplitude and phase of the visible lineshape for each mode and correct the vibrational spectrum from the Φ-dependent terms in Eq. (16). This supposes that a starting point for the values of resonance frequencies ω_l is provided to the fitting algorithm. Of course these may be estimated from the spectra, but interference with a nonresonant background[50] or between nearby modes frequently may make it difficult to determine ω_l without curve fitting. The optimal solution is probably to perform a first simplified fit to get the starting ω_l values. It is conceivable to fit with Lorentzians amplitudes independent from the energies, but their unknown phases remain a problem. Another solution lies in replacing the exact Eq. 12 by its value at peak maximum $\widetilde{D}_l = \frac{\Delta_l}{2}\left[\Phi(\omega_{SFG}) - \Phi(\omega_{vis})\right]$, which becomes identical for all modes and may be factorized. A comparison of both D_l and $\widetilde{D}_l$ functions in Fig. 1 shows that, for standard experimental conditions, their difference reaches at maximum 6% in magnitude and 3° in phase at 50 cm^{-1} distance from the vibration maximum (i.e. far beyond the homogeneous vibrational linewidth Γ_l, usually a few wavenumbers). We therefore suggest to first fit the spectra using the peak maximum $\widetilde{D}_l$ function, then turn to the full D_l for final convergence of the fit.

The values of $\left|\chi^l_{yzy}\right| = \left|\chi^l_{zyy}\right|$ and $\left|\chi^l_{yyz}\right| = \dfrac{\sin^2\theta}{2\cos^2\theta}\left|\chi^l_{zzz}\right|$ are now known from curve fitting of sps and ssp spectra after proper account of the local field factors, but not their signs. As is usually done, those may be obtained from heterodyne measurements[77–79], or from the interference with a nonresonant contribution of known phase (e.g. gold[80,81]). The overall consistency may then be checked by comparing the ppp spectrum calculated from the linear combination of the four previous tensor components to the experimental spectrum. Once these signed quantities are known for each mode l, so are the left sides of Eq. 24 and 25, providing useful information.

If Eq. 24 vanishes, it means that vibration mode l is perpendicular to c axis. If Eq. 25 vanishes, mode l should be aligned along c, except for very unlikely situations (e.g. mode l aligned along b and $\psi = 0$). In the general case, we first suppose that there is at least one mode, called $l = ref$, for which neither of these equations vanish, and that quantities $\left(\frac{\partial \mu^c}{\partial Q_{ref}}\right)_0$ and $\left(\frac{\partial \mu^\perp}{\partial Q_{ref}}\right)_0$ (i.e. IR activities parallel and perpendicular to the electronic transition moment) are known (or at least their ratio) from the molecular model. We note that these quantities may also stem from polarized infrared absorption spectroscopy experiments,

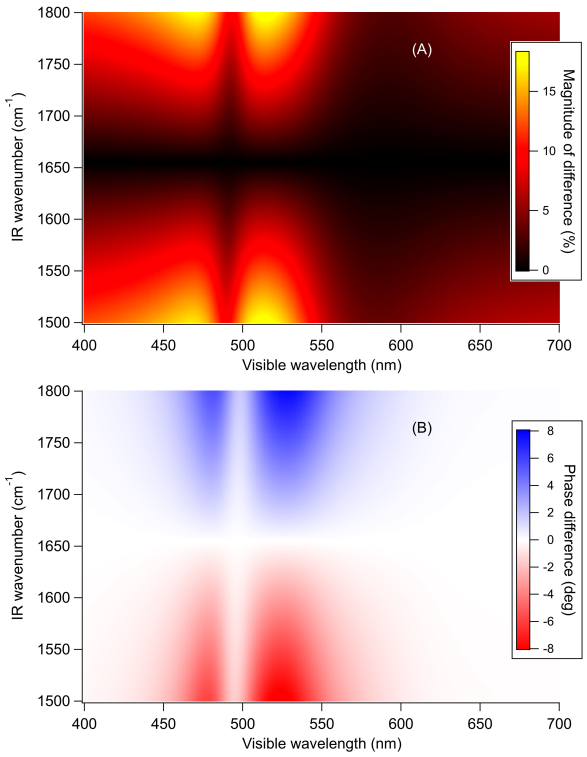

FIG. 1. Relative difference in amplitude (A) and phase difference (B) between functions D_l and $\widetilde{D}_l$, using Φ function calculated from the absorption spectrum of a 10^{-4}M rhodamine 123 solution[17] and $\omega_l = 1655$ cm^{-1}.

but those usually do not succeed in extracting a measurable signal at the monolayer level, hence the resort to SFG spectroscopy. Performing such an assignment of DR-SFG experimental vibration modes to specific modes of the molecular model supposes that they may be unambiguously identified and separated. Considering the usually complex molecular structure of chromophores, one should avoid focusing on a crowded or unspecific vibrational range (e.g. CH stretch region for aliphatic chains) and rather turn to the fingerprint region.[27,79] Taking this ref mode as the reference, we fix axis (a) along its vibrational transition dipole moment perpendicular to (c) (i.e. we assign it to the (a,c) plane), leading to $\left(\frac{\partial \mu^{\psi}}{\partial Q_{ref}}\right)_0 = \left(\frac{\partial \mu^{\perp}}{\partial Q_{ref}}\right)_0 \cos\psi$, and dividing Eq. 25 by Eq. 24 provides $\cos\psi$. This leaves two possible orientations for the molecule with opposite values of ψ, discriminated by either steric hindrance, optimal chemical interaction with the surface or SFG analysis of another vibration mode not parallel to (a). At this stage, the molecular model and its (a,b,c) frame is fixed on the surface. The hard point for the extension to other vibration modes lies in the

proportionality of Eq. 24 and 25 to Δ_l, so that absolute DR-SFG amplitudes depend on the product of an infrared transition moment by Δ_l. Nevertheless, if the molecular model gives access to the infrared dipole moments projected onto (c) axis, Eq. 24 allows determining the signed ratios of all Δ_l to that of the reference mode Δ_{ref}, including modes for which Eq. 25 vanishes. For modes l with vanishing $\left(\frac{\partial \mu^c}{\partial Q_l}\right)_0$, the knowledge of $\left(\frac{\partial \mu^\perp}{\partial Q_l}\right)_0$ (i.e. the full IR dipole moment) and its angle with the (a) axis is sufficient to calculate Δ_l/Δ_{ref}.

If no ref mode can be found, it means that all probed modes in the DR-SFG spectrum vibrate strictly either parallel or perpendicular to (c), potentially as a consequence of molecular symmetry.[68] There is here no simple way to calculate angle ψ: transitions moments along (c) are not correlated to those in the (a,b) plane anymore, as comparing them requires to analyze two modes (instead of one) and consequently involves the unknown ratio of their Δ_l. For two modes parallel to (c), we may anyway follow the same analysis as above, using Eq. 24 to determine their Δ_l ratio from the projections along (c) only of their infrared dipole moments $\left(\frac{\partial \mu^c}{\partial Q_l}\right)_0$. This method is also valid for two modes perpendicular to (c) and vibrating parallel to each other. Finally, only the situation of two non-parallel modes in the (a,b) plane and no ref mode may be assigned leads to the impossibility to get straightforward information on their Δ_l ratio. To conclude, for most cases, it is possible to determine the relative FC activities (i.e. signed Δ_l) of vibration modes using the experimental DR-SFG data and a small amount of parameters stemming from a simple molecular model.

B. Mixed FC and HT active modes

For a HT mode, several simplifying factors introduced in the FC case disappear. The visible lineshapes (D_l, $E_{1,l}$ and $E_{2,l}$) in Eq. 16 may not be factored anymore, making the curve fitting procedure more complex. However, when i=j (i.e. for xxz, yyz and zzz terms), we may group the $\alpha\beta\gamma$ and $\beta\alpha\gamma$ coefficients to get:

$$\chi^{(2)}_{iik} = \frac{N_s}{\varepsilon_0 \hbar^2} \sum_l \frac{E_l(\omega_{SFG})}{\omega_{IR} - \omega_l + i\Gamma_l} \sum_{\alpha \leq \beta, \gamma} \langle D_{i\alpha} D_{i\beta} D_{k\gamma} \rangle B_l^{\alpha\beta\gamma} \tag{27}$$

with

$$B_l^{\alpha\beta\gamma} = \left[\mu_{eg}^{0,\alpha} \left(\frac{\partial \mu_{eg}^{\beta}}{\partial Q_l}\right)_0 + \left(\frac{\partial \mu_{eg}^{\alpha}}{\partial Q_l}\right)_0 \mu_{eg}^{0,\beta} \right] \left(\frac{\partial \mu^{\gamma}}{\partial Q_l}\right)_0 \text{ for } \alpha \neq \beta, \tag{28}$$

$$B_l^{\alpha\alpha\gamma} = \mu_{eg}^{0,\alpha} \left(\frac{\partial \mu_{eg}^{\alpha}}{\partial Q_l} \right)_0 \left(\frac{\partial \mu^{\gamma}}{\partial Q_l} \right)_0 \tag{29}$$

and

$$E_l\left(\omega_{SFG}\right) = -\frac{\hbar}{2\omega_l}\left[\Phi\left(\omega_{SFG}\right) + \Phi\left(\omega_{SFG} - \omega_l\right)\right] \tag{30}$$

This shows that, for ssp polarization combination (i.e. yyz tensor component), the visible lineshape of a HT mode follows a $E_l(\omega)$ profile rather than a $D_l(\omega)$ one. It is therefore possible to use this particular configuration as a clear marker of the FC or HT nature of a given mode. For conventional singly resonant vibrational SFG, it is sometimes not possible to record ssp signals due to strong screening of the s-polarized beams at the interface as a consequence of high refractive index of the substrate (e.g. metals, silicon) in this range. It is conceivable that the SFG enhancement due to double resonance will compensate for this and make ssp signals measurable. If not, then we may anyway rely on ppp configuration for the following reasons. First, xxz and zzz terms follow the same $E_l(\omega)$ or $D_l(\omega)$ profiles as ssp. For the two remaining components (xzx and zxx), we may consider the following situations for their local field factors: for substrates with a high refractive index in the IR (e.g. a metal), they become negligible as compared to xxz and zzz[80,82]; for substrates with a high refractive index in the visible range (e.g. silicon), the zzz component alone dominates.[83] Consequently, in all situations where ssp spectra may not be recorded, the ppp configuration will involve only components which also follow the $E_l(\omega)$ versus $D_l(\omega)$ profiles for HT versus FC modes, respectively. The discussion below about Fig. 2 shows that is therefore always possible to discriminate the nature of a vibration mode by recording either ssp (low refractive index substrate) or ppp (high refractive index substrate) polarization combination while tuning the visible wavelength.

Components zxx and xzx become important in ppp spectra for substrates with a low refractive index in both visible and infrared ranges (e.g. water, glass). In this situation, as the local field factors for zxx and xzx only differ by the angles of incidence and dispersion of the refractive index at the visible and SFG wavelengths, it may be shown that they almost coincide.[84] Consequently, zxx and xzx terms sum up (with a sign difference[19]), and we may

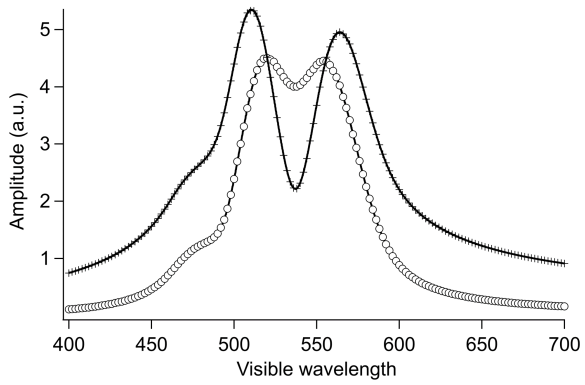

FIG. 2. Amplitudes of D_l (line with open dots) and E_l (line with crosses) functions at vibration peak maximum, using Φ function calculated from the absorption spectrum of a 10^{-4}M rhodamine 123 solution[17] and $\omega_l = 1655$ cm^{-1}.

group them into

$$\chi^{(2)}_{zxx} - \chi^{(2)}_{xzx} = \frac{N_s}{\varepsilon_0 \hbar} \frac{1}{\Delta_l \omega_l} \sum_l \frac{D_l(\omega_{SFG})}{\omega_{IR} - \omega_l + i\Gamma_l} \times \sum_{\alpha\beta\gamma} \langle D_{x\alpha} D_{z\beta} D_{x\gamma} \rangle \left[\mu^{0,\alpha}_{eg} \left(\frac{\partial \mu^{\beta}_{eg}}{\partial Q_l} \right)_0 - \left(\frac{\partial \mu^{\alpha}_{eg}}{\partial Q_l} \right)_0 \mu^{0,\beta}_{eg} \right] \left(\frac{\partial \mu^{\gamma}}{\partial Q_l} \right)_0 . \quad (31)$$

Summarizing the results above, we conclude that the visible lineshape of vibration mode l depends on the nature of the mode, on the polarization combination experimentally recorded and on the nature of the substrate. All FC modes will share the $D_l(\omega_{SFG})$ lineshape (Eq. 12). For HT modes, the amplitudes follow the $E_l(\omega_{SFG})$ for ssp polarizations, as well as for ppp polarizations on high refractive index materials. In other cases, including sps and pss polarizations, the total lineshape is a mixture of $D_l(\omega_{SFG})$ and $E_l(\omega_{SFG})$ functions. This difference between D_l and E_l for FC and HT modes, respectively, was already present in an alternate form in Eq. (32b) and (37) of Ref. 52, or in Eq. (6) and (7) of Ref. 26. At this point we have made no hypothesis on the symmetry of the molecule, whose existence may lead to vanishing of some $\beta_{\alpha\beta\gamma}$ terms (on the condition that (a,b,c) coincide with the symmetry axes or planes), simplifying the equations and favouring either D_l or E_l contributions to the visible lineshapes.

In Fig. 2, we plot the evolution of the amplitudes of the $D_l(\omega)$ and $E_l(\omega)$ lineshapes in a hypothetical situation where function Φ is obtained from the absorption spectrum of a rhodamine 123 solution. Inhomogeneous broadening is smaller than in a thin film and the

main peak is rather well defined. As a result, both $D_l(\omega)$ and $E_l(\omega)$ show two interfering peaks as is classically seen in such simulations.[28] The differences relate essentially to the interference pattern between the peaks. For E_l, destructive interference pushes the two maxima far from each other, with a deep and steep valley in between. Conversely, the constructive interference in D_l generates two close peaks with a very small valley between them. Finally, the external tails extend further for function E_l than for D_l. We see that these trends completely match the simulations of Fig. S1 in Ref. 45. In the simulated ssp spectral evolution of the five high energy vibration modes, the two FC and three HT modes (comparing for example the 1657 and 1621 cm^{-1} modes) show the characteristic features described here. Of course, in the adsorbed monolayer case, Φ function is broadened by inhomogeneous broadening in the films and shifted by aggregation.[17]

We compare in Fig. 3 the amplitude and phase of the same lineshapes calculated from three distinct Φ functions: a single lorentzian peak (i.e. without any vibronic tail), the function extracted from the absorption spectrum of rhodamine 123 in solution as in Fig. 2, and from a J–aggregated film of the same molecules deposited on glass from a 10^{-4}M solution.[17] Apart from the differences listed above, we recover the fact that the two peaks of the FC D_l lineshape overlap and merge into one central broad peak when the width of the Φ function grows as a consequence of inhomogeneous broadening. This is less obvious as far as E_l is concerned, because of the destructive interference which keeps both maxima separated although less visible. The other main difference lies in the phases of the functions. Both excitation functions have a zero phase at low energy but, as energy increases, the phase shifts for E_l-driven peaks result in a sign change after crossing the resonance (as is expected from a resonant Lorentzian behaviour), whereas for D_l-driven ones the original vanishing phase is recovered at high energy. This has important consequences on the fitting procedure of the vibrational spectra because the FC and HT modes will not share a common phase during curve fitting.[50] This phase may be predicted for modes belonging to either the D_l or E_l family, but is difficult to estimate beforehand for modes and experimental conditions where D_l and E_l behaviours mix.

The simulations in Fig. 2 and 3 are very general and illustrate the trends that one expects at the lowest order of perturbation[48,49] for a generic vibration mode of a chromophore in solution or in a thin film, as a monomer or in an aggregate, as long as there is only one allowed electronic transition involved in the probed visible range. They show that the clear

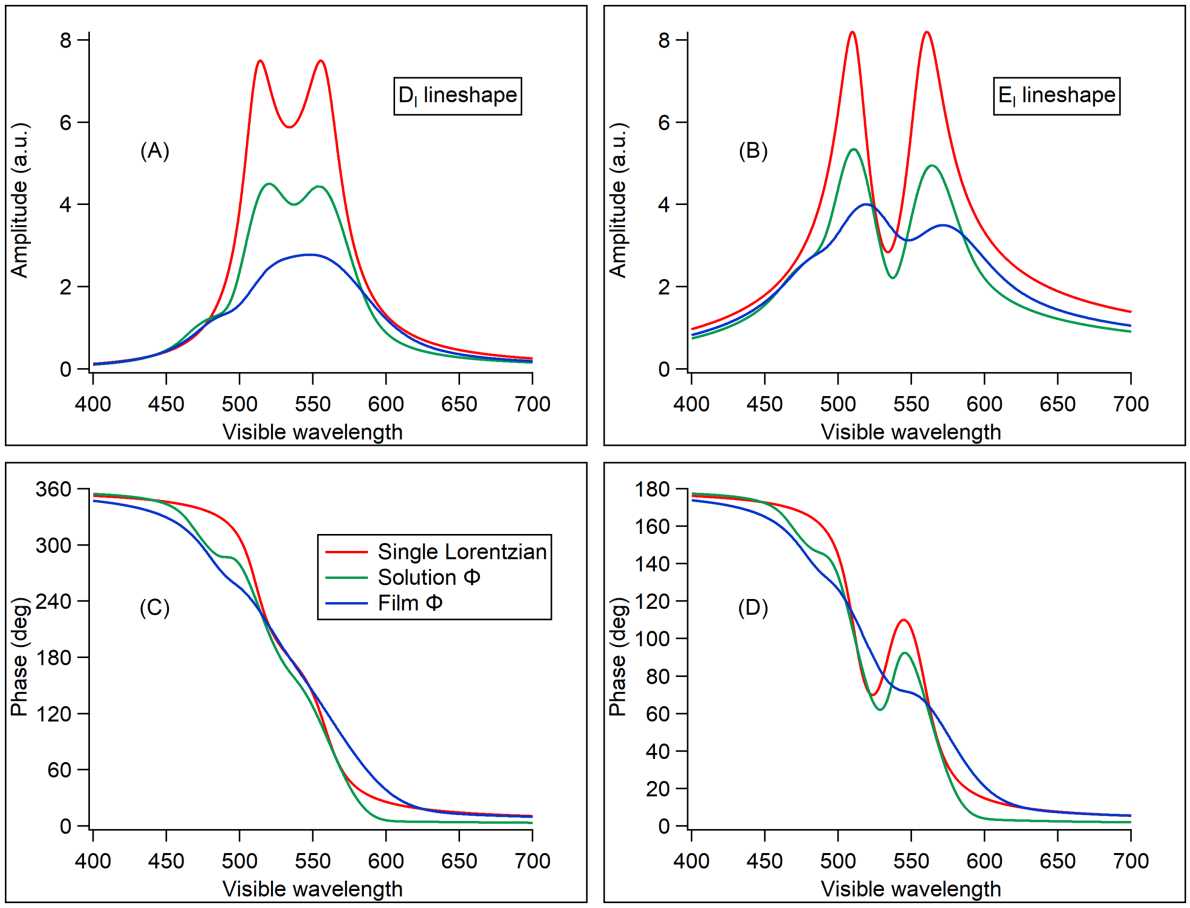

FIG. 3. Comparison of D_l (A–C) and E_l (B–D) lineshapes at vibration peak maximum, in amplitude (A-B) and in phase (C-D), using Φ functions calculated from a single Lorentzian (red), the absorption spectrum of a 10^{-4}M rhodamine 123 solution (green) or the absorption spectrum of a J–aggregated film[17] (blue) and $\omega_l = 1655$ cm^{-1}.

differences between $E_l(\omega)$ and $D_l(\omega)$ profiles allow indeed to discriminate the FC or HT nature of a given mode by recording its experimental excitation profile. As an example, we consider the vibration mode at 1621 cm^{-1} in the vibronic structure of rhodamine 6G (R6G), which is known, together with the intense 1535 cm^{-1} mode, to have HT-activity.[85,86] However, the experimental DR-SFG visible lineshape of this 1621 cm^{-1} mode, recorded on glass using ssp polarisation combination, does not reproduce the expected $E_l(\omega)$ behavior of a HT mode (the lineshape of the 1535 cm^{-1} mode is not provided).[28] Instead, the published excitation profiles are identical for all vibration modes in the DR-SFG spectrum and follow from D_l functions characteristic of FC modes (the reason why there is only one peak showing up instead of two has already been discussed[17] and may be understood from the difference

between red and blue curves in Fig. 3). In addition, all modes appear to share a common phase when spectra are fitted. This is coherent with the methodology supported by Fig. 1 for FC modes, whereas HT modes should strongly differ as for their phases as shown in Fig. 3. For all these reasons, we believe that all modes probed in the original publication[28] are indeed FC-active. An alternate explanation is provided in Ref. 45 by TD-DFT calculations on R6G monomers, showing that a HT-activity of the 1621 cm^{-1} mode is still compatible with the experimental DR-SFG data. We suggest that aggregation is the key parameter to discriminate between both proposals.

As monomers, the vibronic structure of R6G is now well-known and the vibronic activities of the modes originate in the C_s symmetry of the lowest energy conformation of the molecule, which clearly separates vibration modes into totally symmetric and antisymmetric, from which their FC and HT natures follow, respectively.[86] However, contrary to the dilute phase or to low density adsorbates, rhodamine molecules in absorbed monolayers interact to form aggregates,[17,87,88] in which the geometry, electronic structure and symmetry properties of the molecules differ from the monomeric state. It has been shown that the orientation angle of the electronic transition moment in H-aggregates of R6G films may vary from the monomeric value by 30 to 40°.[73] Specifically, the free rotation around the C–C bond between the xanthene ring and the ethoxycarbonylphenyl group may lead to a tilt angle between these moieties differing from the predicted 90°, and accordingly to a C_1-symmetry molecule. In this case, all modes, including that at 1621 cm^{-1}, which in the literature is attributed to either the ethoxycarbonylphenyl group[28,89] or the xanthene skeleton,[45] exhibit FC activity due to the absence of molecular symmetry. In addition, the symmetries of the electron density of a multimer in the ground and excited states differ from the isolated molecule, and so do the electronic levels involved in the electronic transition.[87,88] This modification of the symmetries, together with the change in the orientation of the electronic transition dipole moment, will have a strong impact on the FC or HT nature of each vibration mode.[33] In Ref. 28, the shape, width and redshifted wavelength of the maximum in the film absorbance spectrum favours the formation of J-aggregates, as expected from the concentration used to prepare the films.[88] Experimental data therefore suggest that all modes become FC-active in this case as a consequence of aggregation. This would also account for the fact that the 1621 cm^{-1} mode shows a DR-SFG intensity in the same order of magnitude as the other modes.

IV. CONCLUSION

The experimental and theoretical complexity of DR-SFG experiments should not discourage experimenters to apply this powerful technique to their research, as a thorough data analysis proves rewarding and provides original results. Following previous work, we have shown in this article that it is indeed possible, proceeding step by step, to disentangle the various parameters involved in DR-SFG spectra: vibrational curve fitting, lineshape in the visible range, orientation of molecules in the sample, FC versus HT natures of the vibration modes. The FC or HT natures of the modes follow from the experimental visible lineshapes. Depending on the nature of the substrate, the evolution of the SFG signals as a function of the visible wavelength either in ssp or ppp configuration is sufficient for this discrimination. The overlap spectral function Φ, extracted from experimental data as explained before,[17] serves as a basis for the following steps. For the main modes, of FC natures, a vibrational curve fitting, performed in two steps, first with an average constant amplitude, then with the full non-constant one, allows to correctly account for the wavelength-dependent parts of the vibrational amplitudes and separate them from the geometrical parameters. Elementary relations between the various susceptibility tensor components, directly following from the double resonant nature, and pinned onto the axes of a molecular model along the electronic and vibrational transition dipole moments, allow to perform an orientation analysis and determine tilt and twist angles. Finally, additional experimental input, either from linear optical absorption spectroscopies in the visible and the infrared ranges or from first principle calculations on the molecular model, may lead to the separation between molecular infrared and visible transition moments on one side, and FC activities on the other side, finalizing the full data analysis.

ACKNOWLEDGMENTS

We thank Prof. Dennis Hore (University of Victoria, Canada) for his fruitful comments on this work and his suggestions to improve this manuscript.

DATA AVAILABILITY

Data sharing is not applicable to this article as no new data were created or analyzed in this study.

Appendix: FC and HT contributions to DR-SFG

In order to compare the FC and HT terms of the DR-SFG hyperpolarizability using a common formalism, we briefly recall their origins. A harmonic vibration mode (l) is defined by its resonant frequency ω_l, width Γ_l, and normal coordinate Q_l. The harmonic potential energy curves along normal coordinate Q_l for ground and excited (e) states are shifted by Δ_l, so that $Q_l^e = Q_l + \Delta_l$. The total SFG hyperpolarizability breaks down into excitations of these vibration modes by the IR photon (ω_{IR}), scaled by their IR activity $\left(\frac{\partial \mu^\gamma}{\partial Q_l}\right)_0$:[48]

$$\beta_{\alpha\beta\gamma} = 1/\hbar^2 \sum_l \frac{\left(\frac{\partial \mu^\gamma}{\partial Q_l}\right)_0 \sqrt{\frac{\hbar}{2\omega_l}}}{\omega_{IR} - \omega_l + i\Gamma_l} \sum_{\{u\}} \frac{\mu^\alpha_{g0\leftarrow eu}\ \mu^\beta_{eu\leftarrow gl}}{\omega_{SFG} - \omega_{eug0} + i\Gamma_{eg}}, \tag{A.1}$$

where μ is the dipole moment, $\{u\}$=$\{j, u_j\}$ spans the vibronic modes, $\hbar\omega^0_{eg}$ is the vibrationless electronic transition energy, $\hbar\omega_{eug0} = \hbar\omega^0_{eg} + \sum_j u_j \hbar\omega_j$ is the vibronic energy, $\mu^\alpha_{g0\leftarrow eu}$ and $\mu^\beta_{eu\leftarrow gl}$ represent the dipolar transition moments between ground (g, vibrational state $l = 0$ or $l = 1$) and excited electronic states (e, vibrational state u).

Expanding the energy denominators into complex exponential terms using

$$\frac{1}{\omega_{SFG} - \omega_{eug0} + i\Gamma_{eg}} = \frac{1}{i}\int_0^\infty dt\, e^{it\left(\omega - \omega^0_{eg} + i\Gamma_{eg}\right)} \prod_j e^{-iu_j\omega_j t} \tag{A.2}$$

leads to

$$\beta_{\alpha\beta\gamma} = 1/\hbar^2 \sum_l \frac{\left(\frac{\partial \mu^\gamma}{\partial Q_l}\right)_0}{\omega_{IR} - \omega_l + i\Gamma_l} \mathcal{F}_l^{\alpha\beta}(\omega_{SFG}) \tag{A.3}$$

with

$$\mathcal{F}_l^{\alpha\beta}(\omega) = (-i)\sqrt{\frac{\hbar}{2\omega_l}} \int_0^\infty dt\, e^{it\left(\omega - \omega^0_{eg} + i\Gamma_{eg}\right)} \sum_{\{u\}} \mu^\alpha_{g0\leftarrow eu}\ \mu^\beta_{eu\leftarrow gl} \prod_j e^{-iu_j\omega_j t}, \tag{A.4}$$

Assuming Born-Oppenheimer approximation allows separating the electronic and vibrational parts of the wavefunctions ψ, and Eq. 5 leads to a straightforward integration along the electronic wavefunctions. For the vibrational part, we have:

$$\mu^{\alpha}_{g0\leftarrow eu} = \mu^{0,\alpha}_{eg} \left\langle \psi^{vib,g}_{0} \middle| \psi^{vib,e}_{u} \right\rangle + \sum_{a} \left(\frac{\partial \mu^{\alpha}_{eg}}{\partial Q_a} \right)_0 \left\langle \psi^{vib,g}_{0} \middle| Q_a \middle| \psi^{vib,e}_{u} \right\rangle \tag{A.5}$$

$$\mu^{\beta}_{eu\leftarrow gl} = \mu^{0,\beta}_{eg} \left\langle \psi^{vib,e}_{u} \middle| \psi^{vib,g}_{l} \right\rangle + \sum_{b} \left(\frac{\partial \mu^{\beta}_{eg}}{\partial Q_b} \right)_0 \left\langle \psi^{vib,e}_{u} \middle| Q_b \middle| \psi^{vib,g}_{l} \right\rangle \tag{A.6}$$

Product $\mu^{\alpha}_{g0\leftarrow eu}\mu^{\beta}_{eu\leftarrow gl}$ therefore comprises four generic terms, each weighted by $\mu^{0,\alpha}_{eg}\ \mu^{0,\beta}_{eg}$, $\mu^{0,\alpha}_{eg}\left(\frac{\partial \mu^{\beta}_{eg}}{\partial Q_b}\right)_0$, $\left(\frac{\partial \mu^{\alpha}_{eg}}{\partial Q_a}\right)_0 \mu^{0,\beta}_{eg}$ and $\left(\frac{\partial \mu^{\alpha}_{eg}}{\partial Q_a}\right)_0 \left(\frac{\partial \mu^{\beta}_{eg}}{\partial Q_b}\right)_0$, giving rise to FC, HT1, HT2 and HT3 contributions, respectively. HT1 and HT2 are sometimes referred to as FC-HT interference terms[43] whereas HT3 is a pure HT contribution. We recover here the amplitudes defined in Eq. 6 to 9. The excitation spectra D_l and $E_{1/2/3,l}$ all have the same functional form:

$$(-i)\sqrt{\frac{\hbar}{2\omega_l}} \int_0^{\infty} dt\, e^{it\left(\omega-\omega^0_{eg}+i\Gamma_{eg}\right)} \sum_{\{u\}} \left\langle \psi^{vib,g}_{0} \middle| f(Q_a) \middle| \psi^{vib,e}_{u} \right\rangle \left\langle \psi^{vib,e}_{u} \middle| f(Q_b) \middle| \psi^{vib,g}_{l} \right\rangle \prod_j e^{-iu_j\omega_j t} \tag{A.7}$$

where $f(Q_j)$ equals 1 for $j \neq \{a,b\}$, and either 1 or $Q_{a/b}$ for $j = \{a,b\}$ to generate the four contributions. The summation over the vibronic structure $\{u\}$ may be explicitly performed using the following procedure:

– transform the vibrational overlap into a product of two integrals over Q_j and $\widetilde{Q}_j$ by introducing Hermite polynomials (H_p), in particular:

$$\psi^{vib,e}_{u} = \prod_j \frac{1}{\sqrt{2^{u_j} u_j!}} \left(\frac{\omega_j}{\hbar\pi}\right)^{1/4} H_{u_j}\left(\sqrt{\frac{\omega_j}{\hbar}} Q^e_j\right) e^{-\frac{\omega_j}{2\hbar}\left(Q^e_j\right)^2}; \tag{A.8}$$

with

$$\left\langle \psi_1(Q) \middle| f(Q) \middle| \psi_2(Q) \right\rangle = \int_{-\infty}^{\infty} \psi_1(Q)\psi_2(Q)f(Q)dQ \tag{A.9}$$

– perform summation over {uj} by use of Mehler formula[90] for Hermite polynomials

$$\sum_{u_j=0}^{\infty} \frac{H_{u_j}(\alpha)H_{u_j}(\beta)}{u_j!}\left(\frac{w_j}{2}\right)^{u_j} = \frac{1}{\sqrt{1-w_j^2}} exp\left(\frac{2\alpha\beta w_j - \left(\alpha^2+\beta^2\right)w_j^2}{1-w_j^2}\right) \tag{A.10}$$

with $w_j = e^{-i\omega_j t}$;

– after expanding the integral expressions over variables Q_j and $\widetilde{Q}_j$ and setting new integration variables[49] to $x_j = Q^e_j + \widetilde{Q}^e_j = Q_j + \widetilde{Q}_j + 2\Delta_j$ and $y_j = Q^e_j - \widetilde{Q}^e_j = Q_j - \widetilde{Q}_j$,

all integrals simplify into

$$(-i)\int_0^\infty dt\, e^{it\left(\omega-\omega_{eg}^0+i\Gamma_{eg}\right)}\prod_j \frac{\omega_j}{2\pi\hbar}\frac{1}{\sqrt{1-w_j^2}}e^{-\frac{\omega_j\Delta_j^2}{\hbar}}I_{xy} \tag{A.11}$$

with

$$I_{xy}=\int_{-\infty}^{\infty}\int_{-\infty}^{\infty} dx_j dy_j f(Q_j)f(\widetilde{Q}_j)\widetilde{Q}_l e^{-\frac{\omega_j}{2\hbar}\left(\frac{y_j^2}{1-w_j}+\frac{x_j^2}{1+w_j}+2x_j\Delta_j\right)} \tag{A.12}$$

– the integrals over x_j and y_j separate, and each of them is a linear combination of Gaussian integrals I_n, where

$$I_n=\int_{-\infty}^{\infty} u^n e^{-\beta u^2+\gamma u}\, du \tag{A.13}$$

where $\beta_x=\frac{\omega_j}{2\hbar}\frac{1}{1+w_j}$ and $\gamma_x=\frac{\omega_j\Delta_j}{\hbar}$ for x_j integrals, $\beta_y=\frac{\omega_j}{2\hbar}\frac{1}{1-w_j}$ and $\gamma_y=0$ for y_j integrals. The values of I_n are known, and we get $I_n=\widetilde{I}_n I_0$, with

$$I_0=\sqrt{\frac{\pi}{\beta}}e^{\frac{\gamma^2}{4\beta}}\ ;\ \widetilde{I}_1=\frac{\gamma}{2\beta}\ ;\ \widetilde{I}_2=\frac{\gamma^2+2\beta}{4\beta^2}\ ;\ \widetilde{I}_3=\frac{\gamma^3+6\beta\gamma}{8\beta^3} \tag{A.14}$$

– setting $I_0(x_j)I_0(y_j)=\frac{2\pi\hbar\sqrt{1-w_j^2}}{\omega_j}e^{\frac{\omega_j\Delta_j^2}{2\hbar}(1+w_j)}$ as a common factor simplifies the expressions for the excitation spectra into

$$(-i)\int_0^\infty dt\, e^{it\left(\omega-\omega_{eg}^0+i\Gamma_{eg}\right)}\prod_j g_j(t)\mathcal{H}(t) \tag{A.15}$$

where $\mathcal{H}(t)$ is the product of linear combinations of factors $\widetilde{I}_1$, $\widetilde{I}_2$, $\widetilde{I}_3$ for mode l and, if relevant, modes a and b; $g_j(t)=e^{-S_j(1-w_j)}$ and $S_j=\frac{\omega_j\Delta_j^2}{2\hbar}$;

– it becomes possible to recast the expressions in terms of function $\Phi(\omega)$, considering that

$$\Phi(\omega)=i\int_0^\infty dt\, e^{it\left(\omega-\omega_{eg}^0+i\Gamma_{eg}\right)}\prod_j g_j(t) \tag{A.16}$$

and that each w_j term in $\mathcal{H}(t)$ shift the argument of Φ by $-\omega_j$.

With this procedure, all the terms are easily calculated by selecting the process (FC, HT1, HT2 or HT3), replacing functions $f(Q_a)$ and $f(Q_b)$ by their values in Eq. A.7 and A.12, transforming the integrand using x and y variables, separating the terms into I_n integrals,

integrating them into function $\mathcal{H}(t)$ by use of Eq. A.14, and recasting the result in terms of function $\Phi(\omega)$ by expanding $\mathcal{H}(t)$ into increasing powers of w_l, w_a and w_b.

As an example, we evaluate the FC term, for which f(Q)=1. The integrand is thus $\widetilde{Q}_l = 1/2(x_l - y_l) - \Delta_l$ and gives, after integration, $\mathcal{H}_{FC}(t) = 1/2\widetilde{I}_1(x_l) - \Delta_l = -\frac{\Delta_l}{2}(1 - w_l)$. Plugging this result in Eq. A.15 allows to recover Eq. 12.

For the HT1 term, we get for the integrand $\widetilde{Q}_l\widetilde{Q}_a$. Care must be taken when integrating to separate the cases $a = l$ and $a \neq l$. For the latter, integrals separate and, from the FC calculation, we deduce immediately that integration leads to $\left(-\frac{\Delta_l}{2}\right)\left(-\frac{\Delta_a}{2}\right)(1 - w_l)(1 - w_a)$. For the situation $a = l$, integrand becomes $\left(\frac{x_l - y_l}{2} - \Delta_l\right)^2$ leading after integration to $1/4\widetilde{I}_2(x_l) + 1/4\widetilde{I}_2(y_l) - \Delta_l\widetilde{I}_1(x_l) + (\Delta_l)^2 = \frac{\hbar}{2\omega_l} + \frac{(\Delta_l)^2}{4}(1 - w_l)^2$. We obtain the same result as for $a \neq l$, with an additional self-coupling term $\frac{\hbar}{2\omega_l}$ specific to mode l. Collating all terms, we find $\mathcal{H}_{HT1}(t) = \left(-\frac{\Delta_l}{2}\right)\left(-\frac{\Delta_a}{2}\right)(1 - w_l)(1 - w_a) + \frac{\hbar}{2\omega_l}\delta_{al}$.

Calculation is almost identical for HT2, using integrand $\widetilde{Q}_l Q_a$. For $a \neq l$, integrand $[1/2(x_l - y_l) - \Delta_l]\,[1/2(x_a + y_a) - \Delta_a]$ separates and gives the same result as for HT1 because $\widetilde{I}_1(y)$ terms vanish. For $a = l$, integration leads to $1/4\widetilde{I}_2(x_l) - 1/4\widetilde{I}_2(y_l) - \Delta_l\widetilde{I}_1(x_l) + (\Delta_l)^2 = \frac{\hbar}{2\omega_l}w_l + \frac{(\Delta_l)^2}{4}(1 - w_l)^2$. Again, the result is identical to HT1, except for the self-coupling term, equal here to $\frac{\hbar}{2\omega_l}w_l$. We finally get $\mathcal{H}_{HT2}(t) = \left(-\frac{\Delta_l}{2}\right)\left(-\frac{\Delta_a}{2}\right)(1-w_l)(1-w_a) + \frac{\hbar}{2\omega_l}w_l\delta_{al}$. These results essentially match those in Ref. 45, which involve the dimensionless shifts $\overline{\Delta}_j = \Delta_j\sqrt{\omega_j^g/\hbar}$.

Finally, for HT3, the integrand is $\widetilde{Q}_l Q_a \widetilde{Q}_b$. The calculation is led in the same way, except that there are five cases to consider, namely $\{a \neq b \neq l\}$, $\{a = b \neq l\}$, $\{a = l \neq b\}$, $\{b = l \neq a\}$, $\{a = b = l\}$. After collating all terms, we recover a generic contribution $\left(-\frac{\Delta_l}{2}\right)\left(-\frac{\Delta_a}{2}\right)\left(-\frac{\Delta_b}{2}\right)(1 - w_l)(1 - w_a)(1 - w_b)$ valid whatever a, b and l, together with additional coupling and self-coupling terms $-\frac{\hbar\Delta_l}{4\omega_a}(1 - w_l)w_a$ for $a = b$, $-\frac{\hbar\Delta_b}{4\omega_l}(1 - w_b)w_l$ for $l = a$, and $-\frac{\hbar\Delta_a}{4\omega_l}(1 - w_a)$ for $l = b$. We may express it in the following way: $\mathcal{H}_{HT3}(t) = \left(-\frac{\Delta_l}{2}\right)\left(-\frac{\Delta_a}{2}\right)\left(-\frac{\Delta_b}{2}\right)(1-w_l)(1-w_a)(1-w_b) - \frac{\hbar\Delta_l}{4\omega_a}(1-w_l)w_a\delta_{ba} - \frac{\hbar\Delta_b}{4\omega_l}(1-w_b)w_l\delta_{al} - \frac{\hbar\Delta_a}{4\omega_l}(1 - w_a)\delta_{bl}$.

REFERENCES

[1]Q.-Q. Zhou, Y.-Q. Zou, L.-Q. Lu, and W.-J. Xiao, Angewandte Chemie International Edition **58**, 1586 (2019).

[2]L. Wei, M. Wei, L. Mengjie, Z. Xiaodan, C. Hongli, and D. Yulin, Nature Comm. **5**, 3208 (2014).

[3]P. K. Jain, J. Phys. Chem. C **123**, 24347 (2019).

[4]J. Luo, S. Zhang, M. Sun, L. Yang, S. Luo, and J. C. Crittenden, ACS Nano **13**, 9811 (2019).

[5]A. Hagfeldt, G. Boschloo, L. Sun, L. Kloo, and H. Pettersson, Chem. Rev. **110**, 6595 (2010).

[6]A. K. Singh, A. Maibam, B. H. Javaregowda, R. Bisht, A. Kudlu, S. Krishnamurty, K. Krishnamoorthy, and J. Nithyanandhan, J. Phys. Chem. C **124**, 18436 (2020).

[7]S. Ye, A. Kathiravan, H. Hayashi, Y. Tong, Y. Infahsaeng, P. Chabera, T. Pascher, A. P. Yartsev, S. Isoda, H. Imahori, and V. Sundström, J. Phys. Chem. C **117**, 6066 (2013).

[8]H. Imahori, S. Kang, H. Hayashi, M. Haruta, H. Kurata, S. Isoda, S. E. Canton, Y. Infahsaeng, A. Kathiravan, T. Pascher, P. Chábera, A. P. Yartsev, and V. Sundström, J. Phys. Chem. A **115**, 3679 (2011).

[9]L. Si and H. He, J. Phys. Chem. A **118**, 3410 (2014).

[10]R. Pandey, A. P. Moon, J. A. Bender, and S. T. Roberts, J. Phys. Chem. Lett. **7**, 1060 (2016).

[11]K. R. Mulhern, M. R. Detty, and D. F. Watson, J. Phys. Chem. C **115**, 6010 (2011).

[12]S. M. Falke, C. A. Rozzi, D. Brida, M. Maiuri, M. Amato, E. Sommer, A. De Sio, A. Rubio, G. Cerullo, E. Molinari, and C. Lienau, Science **344**, 1001 (2014).

[13]S. Ramakrishna, F. Willig, and V. May, Phys. Rev. B **62**, R16330 (2000).

[14]F. Milota, V. I. Prokhorenko, T. Mancal, H. von Berlepsch, O. Bixner, H. F. Kauffmann, and J. Hauer, J. Phys. Chem. A **117**, 6007 (2013).

[15]A. Monti, C. F. A. Negre, V. S. Batista, L. G. C. Rego, H. J. M. de Groot, and F. Buda, J. Phys. Chem. Lett. **6**, 2393 (2015).

[16]S. Sengupta, L. Bromley III, and L. Velarde, J. Phys. Chem. C **121**, 3424 (2017).

[17]B. Busson, M. Farhat, P.-J. Nini-Teunda, S. Roy, T. Jarisz, and D. K. Hore, J. Chem. Phys. **154**, 224704 (2021).

[18]C. M. Johnson and E. Tyrode, Phys. Chem. Chem. Phys. **7**, 2635 (2005).

[19]X. Zhuang, P. B. Miranda, D. Kim, and Y. R. Shen, Phys. Rev. B **59**, 12632 (1999).

[20]E. H. G. Backus, A. Eichler, A. W. Kleyn, and M. Bonn, Science **310**, 1790 (2005).

[21]P. Fischer and F. Hache, Chirality **17**, 421 (2005).

[22]P. Fischer, F. W. Wise, and A. C. Albrecht, J. Phys. Chem. A **107**, 8232 (2003).

[23]M. A. Belkin and Y. R. Shen, Phys. Rev. Lett. **91**, 213907 (2003).

[24]R.-H. Zheng, D.-M. Chen, W.-M. Wei, T.-J. He, and F.-C. Liu, J. Phys. Chem. B **110**, 4480 (2006).

[25]S. H. Han, N. Ji, M. A. Belkin, and Y. R. Shen, Phys. Rev. B **66**, 165415 (2002).

[26]R.-H. Zheng, W.-M. Wei, Y.-Y. Jing, H. Liu, and Q. Shi, J. Phys. Chem. C **117**, 11117 (2013).

[27]M. Okuno, D. Ishikawa, W. Nakanishi, K. Ariga, and T.-a. Ishibashi, J. Phys. Chem. C **121**, 11241 (2017).

[28]M. B. Raschke, M. Hayashi, S. H. Lin, and Y. R. Shen, Chem. Phys. Lett. **359**, 367 (2002).

[29]L. Dreesen, C. Humbert, Y. Sartenaer, Y. Caudano, C. Volcke, A. A. Mani, A. Peremans, P. A. Thiry, S. Hanique, and J.-M. Frère, Langmuir **20**, 7201 (2004).

[30]T. Maeda, T. Nagahara, M. Aida, and T.-a. Ishibashi, J. Raman Spec. **39**, 1694 (2008).

[31]T. Nagahara, K. Kisoda, H. Harima, M. Aida, and T.-a. Ishibashi, J. Phys. Chem. B **113**, 5098 (2009).

[32]T. Miyamae, E. Ito, Y. Noguchi, and H. Ishii, J. Phys. Chem. C **115**, 9551 (2011).

[33]M. Raab, J. C. Becca, J. Heo, C.-K. Lim, A. Baev, L. Jensen, P. N. Prasad, and L. Velarde, J. Chem. Phys. **150**, 114704 (2019).

[34]Q. Li, R. Hua, and K. C. Chou, J. Phys. Chem. B **112**, 2315 (2008).

[35]T. Miyamae, K. Tsukagoshi, and W. Mizutani, Phys. Chem. Chem. Phys. **12**, 14666 (2010).

[36]Y. Caudano, C. Silien, C. Humbert, L. Dreesen, A. A. Mani, A. Peremans, and P. A. Thiry, J. Electron Spectros. Relat. Phenomena **129**, 139 (2003).

[37]K. C. Chou, S. Westerberg, Y. R. Shen, P. N. Ross, and G. A. Somorjai, Phys. Rev. B **69**, 153413 (2004).

[38]B. Bozzini, L. D'Urzo, C. Mele, B. Busson, C. Humbert, and A. Tadjeddine, J. Phys. Chem. C **112**, 11791 (2008).

[39]T. Miyamae, Y. Miyata, and H. Kataura, J. Phys. Chem. C **113**, 15314 (2009).

[40]E. Kakudji, C. Silien, D. Lis, F. Cecchet, A. Nouri, P. A. Thiry, A. Peremans, and Y. Caudano, phys. stat. sol. b **247**, 1992 (2010).

[41]S. Yang, H. Noguchi, and K. Uosaki, J. Phys. Chem. C **119**, 26056 (2015).

[42]D. Elsenbeck, S. K. Das, and L. Velarde, Phys. Chem. Chem. Phys. **19**, 18519 (2017).

[43]D. W. Silverstein and L. Jensen, J. Chem. Phys. **136**, 064111 (2012).

[44]D. W. Silverstein and L. Jensen, J. Chem. Phys. **136**, 064110 (2012).

[45]P. A. Weiss, D. W. Silverstein, and L. Jensen, J. Phys. Chem. Lett. **5**, 329 (2014).

[46]J. Y. Huang and Y. R. Shen, Phys. Rev. A **49**, 3973 (1994).

[47]M. Hayashi, S. H. Lin, M. B. Raschke, and Y. R. Shen, J. Phys. Chem. A **106**, 2271 (2002).

[48]B. Busson, J. Chem. Phys. **153**, 174701 (2020).

[49]B. Busson, J. Chem. Phys. **153**, 174702 (2020).

[50]B. Busson and A. Tadjeddine, J. Phys. Chem. C **113**, 21895 (2009).

[51]T. Azumi and K. Matsuzaki, Photochem. Photobiol. **25**, 315 (1977).

[52]A. Warshel and P. Dauber, J. Chem. Phys. **66**, 5477 (1977).

[53]A. C. Albrecht, J. Chem. Phys. **34**, 1476 (1961).

[54]B. R. Stallard, P. M. Champion, P. R. Callis, and A. C. Albrecht, J. Chem. Phys. **78**, 712 (1983).

[55]J. C. Vallet, A. J. Boeglin, J. P. Lavoine, and A. A. Villaeys, Phys. Rev. A **53**, 4508 (1996).

[56]A. Baiardi, J. Bloino, and V. Barone, J. Chem. Theory Comput. **9**, 4097 (2013).

[57]K. C. Jena, K. K. Hung, T. R. Schwantje, and D. K. Hore, J. Chem. Phys. **135**, 044704 (2011).

[58]S. Roy, K.-K. Hung, U. Stege, and D. K. Hore, Appl. Spectrosc. Rev. **49**, 233 (2014).

[59]B. Busson and L. Dalstein, J. Phys. Chem. C **123**, 26597 (2019).

[60]C. Hirose, N. Akamatsu, and K. Domen, Appl. Spectrosc. **46**, 1051 (1992).

[61]D. K. Hore, D. K. Beaman, D. H. Parks, and G. L. Richmond, J. Phys. Chem. B **109**, 16846 (2005).

[62]K.-K. Hung, U. Stege, and D. K. Hore, Appl. Spec. Rev. **50**, 351 (2015).

[63]M. A. Belkin, Y. R. Shen, and R. A. Harris, J. Chem. Phys. **120**, 10118 (2004).

[64]W. Gan, B.-H. Wu, Z. Zhang, Y. Guo, and H.-F. Wang, J. Phys. Chem. C **111**, 8716 (2007).

[65]A. A. Mani, Z. D. Schultz, Y. Caudano, B. Champagne, C. Humbert, L. Dreesen, A. A. Gewirth, J. O. White, P. A. Thiry, and A. Peremans, J. Phys. Chem. B **108**, 16135 (2004).

[66]Z. Guo, W. Zheng, H. Hamoudi, C. Dablemont, V. A. Esaulov, and B. Bourguignon, Surf.

Sci. **602**, 3551 (2008).

[67]F. Cecchet, D. Lis, J. Guthmuller, B. Champagne, G. Fonder, Z. Mekhalif, Y. Caudano, A. A. Mani, P. A. Thiry, and A. Peremans, J. Phys. Chem. C **114**, 4106 (2010).

[68]C. C. Rich, M. A. Mattson, and A. T. Krummel, J. Phys. Chem. C **120**, 6601 (2016).

[69]J. Wang, Z. Paszti, M. L. Clarke, X. Chen, and Z. Chen, J. Phys. Chem. B **111**, 6088 (2007).

[70]J. Bujdák, N. Iyi, Y. Kaneko, A. Czímerová, and R. Sasai, Phys. Chem. Chem. Phys. **5**, 4680 (2003).

[71]S. Yamaguchi and T. Tahara, J. Phys. Chem. B **108**, 19079 (2004).

[72]T. Zhang, Z.-C. Huangfu, Y. Qian, Z. Lu, H. Gao, and Y. Rao, J. Phys. Chem. C **126**, 2823 (2022).

[73]J. Bujdák and N. Iyi, J. Phys. Chem. B **109**, 4608 (2005).

[74]R. Sasai, T. Fujita, N. Iyi, H. Itoh, and K. Takagi, Langmuir **18**, 6578 (2002).

[75]X. Wei, P. B. Miranda, C. Zhang, and Y. R. Shen, Phys. Rev. B **66**, 085401 (2002).

[76]E. Tyrode, C. M. Johnson, S. Baldelli, C. Leygraf, and M. W. Rutland, J. Phys. Chem. B **109**, 329 (2005).

[77]W.-C. Yang and D. K. Hore, J. Phys. Chem. C **121**, 28043 (2017).

[78]W.-C. Yang, B. Busson, and D. K. Hore, J. Chem. Phys. **152**, 084708 (2020).

[79]C. C. Rich, K. A. Lindberg, and A. T. Krummel, J. Phys. Chem. Lett. **8**, 1331 (2017).

[80]L. Dalstein, A. Revel, C. Humbert, and B. Busson, J. Chem. Phys. **148**, 134701 (2018).

[81]A. Le Rille and A. Tadjeddine, J. Electroanal. Chem. **467**, 238 (1999).

[82]M. A. Hines, J. A. Todd, and P. Guyot-Sionnest, Langmuir **11**, 493 (1995).

[83]C. Humbert, O. Pluchery, E. Lacaze, A. Tadjeddine, and B. Busson, Phys. Chem. Chem. Phys. **14**, 280 (2012).

[84]X. Lu, M. L. Clarke, D. Li, X. Wang, G. Xue, and Z. Chen, J. Phys. Chem. C **115**, 13759 (2011).

[85]C. B. Milojevich, D. W. Silverstein, L. Jensen, and J. P. Camden, J. Am. Chem. Soc. **133**, 14590 (2011).

[86]C. B. Milojevich, D. W. Silverstein, L. Jensen, and J. P. Camden, J. Phys. Chem. C **117**, 3046 (2013).

[87]T. Kikteva, D. Star, Z. Zhao, T. L. Baisley, and G. W. Leach, J. Phys. Chem. B **103**, 1124 (1999).

[88]M. Chapman, M. Mullen, E. Novoa-Ortega, M. Alhasani, J. F. Elman, and W. B. Euler, J. Phys. Chem. C **120**, 8289 (2016).

[89]M. Majoube and M. Henry, Spectrochim. Acta Part A **47**, 1459 (1991).

[90]S. H. Lin, J. Chem. Phys. **44**, 3759 (1966).